Experimental and Numerical Investigation of Levitation Force Parameters of Novel Multisurface Halbach HTS–PMG Arrangement for Superconducting Maglev System

Kemal Ozturk, Antonio Badía-Majós, Murat Abdioglu, Durukan Burak Dilek, and Hasan Gedikli

***Abstract*—We have designed multisurface Halbach high temperature superconductor–permanent magnetic guideway (HTS–PMG) arrangements for magnetically levitated transportation (Maglev) and investigated the static force parameters in addition to the dynamic response characteristics. Three different Halbach HTS–PMG arrangements were used with multisurface (6 HTS, 4 HTS) and single surface (2 HTS) configurations and static and dynamic measurements were carried out in three different field cooling heights (FCHs). The bigger vertical loading capacity and wider loading gap were obtained with multisurface Halbach HTS–PMG arrangements. In addition, nearly four times bigger guidance force values of multisurface arrangements than that of single surface one indicates that the side HTSs in multisurface arrangements make a significant contribution to the guidance force and thus lateral movement stability of Maglev systems. Both the vertical and lateral dynamic stiffness values increased with decreasing FCH and it can be also said that the dynamic stiffness properties of Maglev systems can be enhanced especially in lateral direction by using the multisurface Halbach HTS–PMG arrangements. Understanding of these experimental observations is supported by dedicated theoretical modelling through a 2-D approximation of the system. We show that by using a single material parameter (the critical current density J_c) for the whole superconducting set, one may satisfactorily predict the complete series of experiments. The static and dynamic parameters obtained from this study and the results of dedicated theoretical modeling for single–surface and multisurface HTS–PMG arrangements are thought to be helpful for the researchers working on static and dynamic performances of HTS Maglev systems.**

***Index Terms*—Dynamic response, high temperature superconductor (HTS) magnetically levitated transportation (Maglev), levitation force, multisurface, theoretical modeling, vibration characteristics.**

I. Introduction

INCREASING population in the world and thus increasing demand on transportation have made magnetically levitated transportation (Maglev) systems crucial due to the lower energy consumption and higher speed. In superconducting Maglev systems, the magnetic levitation and guidance forces arise from the electromagnetic interaction between high temperature superconductor (HTS) and permanent magnetic guideway (PMG). Optimum Maglev operation requires higher levitation force with sufficient guidance force for higher carrying capacity and movement stability, respectively. Therefore, the magnetic levitation and guidance forces can be accepted as main performance parameters of the HTS Maglev system. The dynamic vibration parameters are also important for safety of the HTS Maglev vehicle in running operation [1]. In an HTS Maglev system, levitation and guidance forces are directly related to dimension and arrangement of PMs in PMG [2]–[5] and magnetic flux density and magnetic flux gradient of PMG [6]–[9] in addition to some crucial intrinsic characteristics of HTS used in Maglev systems such as flux pinning [10]–[12] and related critical current density [12], [13]. Therefore, many researchers are trying to improve magnetic flux density and distribution of the PMG via optimizing the dimensions and combinations of the PMs [14]–[19] and the structural, electromagnetic and superconducting properties of the superconductors [20]–[22]. In addition, not only experimental investigations are being conducted but also analytical [4], [23]–[25] and numerical [24], [26]–[28] ones in order to support experimental research or to predict and clarify the results of underlying physical phenomena.

Up to now, generally two different types of PMGs have been used in studies named as conventional PMG [6], [15],

Manuscript received April 18, 2021; revised June 23, 2021; accepted August 15, 2021. Date of publication August 24, 2021; date of current version September 15, 2021. This work was supported in part by the Scientific and Technological Research Council of Turkey (TUBITAK—Turkey) under Project 118F426. The work of A. Badía-Majós was supported by the Spanish Agencia Estatal de Investigación and the European FEDER Program under Project ENE2017-83669-C4-1-R and the Gobierno de Aragón under Research Group T54_17R. This article was recommended by Associate Editor M. Zhang. *(Corresponding author: Kemal Ozturk.)*

Kemal Ozturk is with the Department of Physics, Faculty of Science, Karadeniz Technical University, 61080 Trabzon, Turkey (e-mail: kozturk6167@gmail.com).

Antonio Badía-Majós is with the Instituto de Nanociencia y Materiales de Aragón (INMA), CSIC-Universidad de Zaragoza, 50009 Zaragoza, Spain (e-mail: antonio.badia.m@gmail.com).

Murat Abdioglu is with the Department of Mathematics and Science Education, Faculty of Education, Bayburt University, 69000 Bayburt, Turkey (e-mail: muratabdioglu61@gmail.com).

Durukan Burak Dilek and Hasan Gedikli are with the Department of Mechanical Engineering, Faculty of Engineering, Karadeniz Technical University, 61080 Trabzon, Turkey (e-mail: durukanb44@gmail.com; hgedikli@ktu.edu.tr).

Color versions of one or more figures in this article are available at https://doi.org/10.1109/TASC.2021.3106816.

Digital Object Identifier 10.1109/TASC.2021.3106816

[29] and Halbach PMG [7], [18], [30]. The conventional PMG has single-pole on the applied region and is consisted by two or three PMs while Halbach PMG is generally consisted by five PMs with double pole. However, both of them are based on single-surface interaction between the PMG and onboard HTS unit [18], [29]. Although Halbach type single-surface HTS–PMG arrangements are the most used ones and superior to other type single surface HTS–PMG arrangements by means of the magnetic levitation and guidance force capacity, the single-surface HTS–PMG arrangements still cannot provide the desired magnetic levitation and guidance forces for technological applications. In a recent study investigating the effects of multisurface HTS–PMG interaction on radial force and stiffness parameters of a flywheel energy storage system [31], it was observed that the radial magnetic stiffness and radial levitation force in a superconducting magnetic bearing system increased by increasing the permanent magnet number. Although the multisurface arrangements with increasing PM are useful for flywheel energy storage systems, it is not an applicable method for the HTS Maglev systems with thousands of kilometer of railway. That is, the levitation and guidance forces of HTS Maglev systems can be enhanced by increasing the pole number (with increasing the PM number) of the used PMG, but in this case the fabrication cost increases dramatically, since the PMG has to be paved between the cities as thousands of kilometres. Therefore, the loading capacity and movement stability of the HTS Maglev systems should be increased together to increase the efficiency of these systems from the viewpoint of fabrication cost.

Although there are lots of studies in literature focused on enhancing the practical applicability of HTS Maglev systems, the vast majority of these studies use single-surface HTS–PMG arrangements (with one interaction surface between the HTS and PMG units) including Halbach PMG too. As different from the literature, we have proposed a new Halbach HTS–PMG arrangement; in this article, based on multisurface interaction between the Halbach PMG and onboard HTS unit to increase the levitation force, guidance force and the magnetic stiffness of HTS Maglev systems together while decreasing the fabrication cost. Following preliminary work [32], a systematic global investigation that involves a conceptual framework to describe such systems is presented here.

In addition, dynamic response characteristics of novel multisurface Halbach HTS–PMG arrangement such as acceleration, resonance frequency, and dynamic stiffness were measured in this study since these are important parameters for the dynamic stability of HTS Maglev systems. The obtained results of this study on multisurface Halbach HTS–PMG arrangement are thought to be useful for researchers and application engineers who focus on superconducting Maglev systems.

From the theoretical side, a dedicated model has been developed and implemented that allows to explain the physical implications of introducing multisurface arrangements. Numerical simulations based on the simple critical state ansatz (constant critical current density) allow to predict the behavior of the different multisurface arrangements with very reasonable performance.

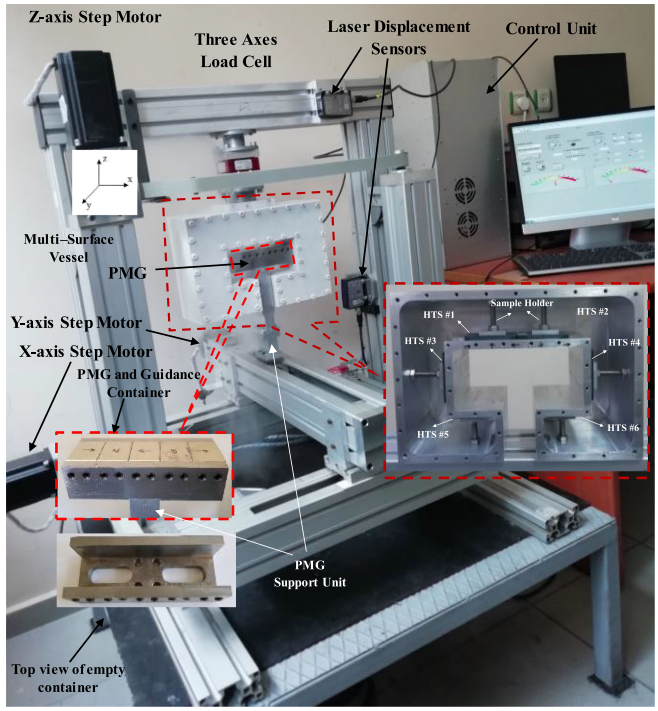

Fig. 1. TAMFS with multisurface Halbach HTS-PMG arrangement.

II. Experimental Procedure

A. Experimental Setup

The levitation force, guidance force and magnetic stiffness performances of the novel multisurface Halbach HTS–PMG arrangement were investigated via the three axes magnetic levitation force measurement system (TAMFS), shown in Fig. 1. The novel multisurface (MS) cryostat in this system allowing up to 6 HTS in it is handmade from aluminum material (6013 series). The movement of the system is provided by three step motors and the displacement is controlled by Baumer OM70 laser displacement sensors in z- and x-axis. The detailed technical specifications of this system can be found in [33]. The Halbach PMG arrangement was constructed in an St37 steel guidance container and the handmade container was fabricated in a single piece from a bulk and the bottom part was carved to utilize from the magnetic flux at the bottom of the PMG as can be seen in Fig. 1. The dimensions and surface magnetic flux densities of each NdFeB (N42) PMs used in Halbach PMG are 40 mm $\times$ 30 mm $\times$ 30 mm and 0.53 T, respectively. The cross section and height of the PMG are 150 $\times$ 30 mm^2 and 40 mm, respectively and detailed information about magnetic flux distribution of a series of Halbach PMGs built with these magnets and alike can be found elsewhere [1], [7]. They support the theoretical analysis performed here.

B. Measurement Procedure

1) Static Measurements: We have used three different Halbach HTS–PMG arrangements as single surface and multisurface with 2 HTS, 4 HTS, and 6 HTS and these arrangements

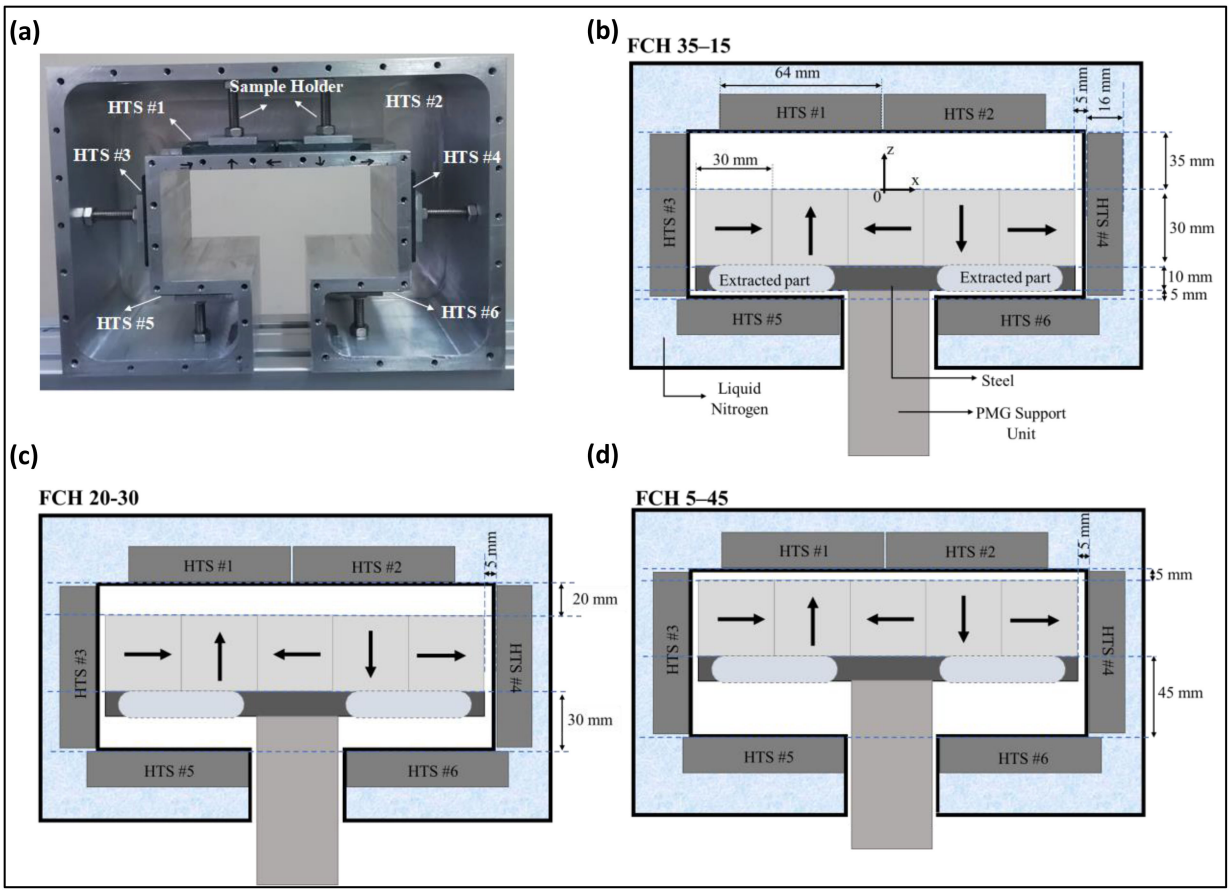

Fig. 2. (a) Inside view from the front surface of novel multisurface cryostat with 6 HTS. (b)–(d) Schematic illustration of different FCHs.

were named as SS–2 HTS (SS: single-surface), MS–4 HTS, and MS–6 HTS (MS: multisurface), respectively. The vertical magnetic levitation force measurements were performed in three different field cooling heights (FCHs) to determine the optimum FCH depending on the flux expulsion and trapping behavior of the HTSs, by taking in mind the geometrical restrictions of the system. Fig. 2(b)–(d) schematically shows different FCHs and the novel multisurface cryostat with 6 HTS is shown in Fig. 2(a). The first number in nomenclatures of FCHs represents the distance between upper surface of the PMG and bottom surface of the upper HTSs (HTS 1 and HTS 2) and the second number represents distance between upper surface of the lower HTSs (HTS 5 and HTS 6) and bottom surface of the PMG. Recall that these numbers always add up 50 mm, which is the full gap in between magnets and superconductors. The HTS 5 and HTS 6 have been removed from the cryostat while constructing MS–4 HTS arrangement and the SS–2 HTS arrangement includes only HTS 1 and HTS 2.

Three-seeded rectangular prism shaped YBCO (YBaCuO) samples (as HTS) with dimensions of 64 mm × 33 mm ×13 mm were provided by ATZ GmbH, Germany. For levitation force measurements in FCH 35–15 case [see Fig. 2(b)], the distance between the upper surface of the PMG and the bottom surface of the upper HTSs (HTS 1 and HTS 2) is fixed at 35 mm before the cooling. Also, the distance between the upper surface of the lower HTSs (HTS 5 and HTS 6) and the bottom surface of the PMG unit with steel part is fixed at 5 mm (and so, the bottom surface of the pure PMG is fixed at 15 mm). The HTSs are cooled in this FCH by filling the vessel with liquid nitrogen (LN2). After completely cooling the HTSs and reaching to the thermal equilibrium, the levitation force is measured while the distance between the upper surface of the PMG and bottom of the upper HTSs is changing from 35 mm (see C1 in Fig. 5) to minimum distance of 5 mm (see C2 in Fig. 5) and again to the initial position of 35 mm (see C3 in Fig. 5). In FCH 20–30 and FCH 5–45 cases, the HTSs are cooled at the related FCHs shown in Fig. 2(c) and (d), respectively. After complete cooling of the HTSs, the levitation force measurements are carried out while the distance between the upper surface of the PMG and bottom of the upper HTSs is changing from related FCH (B1 and A1, respectively for FCH 20–30 and FCH 5–45 cases) to 35 mm, then from 35 mm (B2 and A2) to minimum distance of 5 mm (B3 and A3) and again to 35 mm (B4 and A4). That is, A1, B1, and C1 indicate the initial cooling positions and for clarity, see also the measurement sequences as A1, A2, A3, and A4 for FCH 20–30 and others in Fig. 5.

In the lateral guidance force measurements, the HTSs are cooled in two different FCHs of FCH 5–45 and FCH 20–30. After completely cooling of the HTSs, the vertical distance between the upper surface of the PMG and the bottom of the

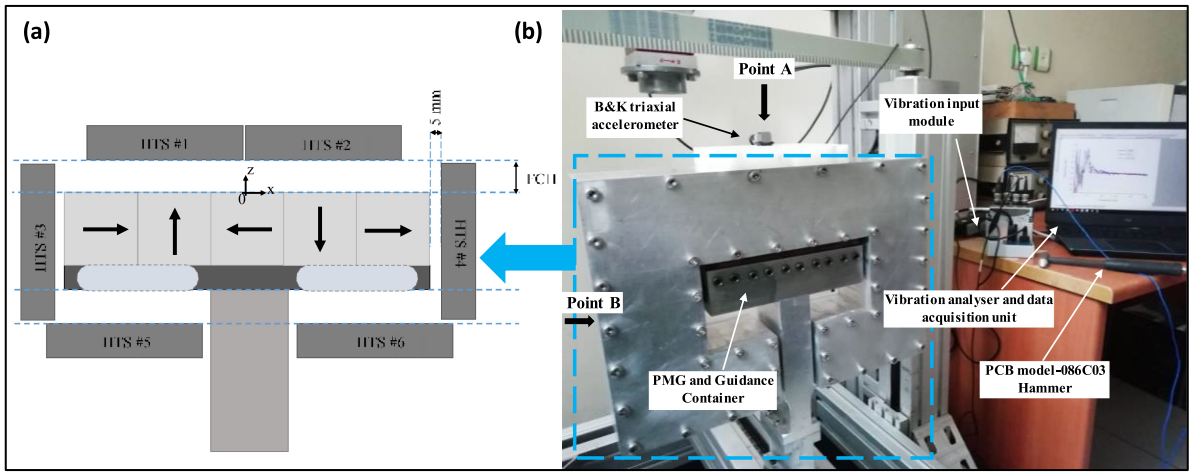

Fig. 3. (a) Schematic view of multisurface HTS–PMG arrangement with 6 HTS for dynamic measurements. (b) Photo of the Dynamic measurement system.

upper HTSs is fixed to the working height (WH) of 20 mm. After this procedure, the lateral guidance force measurements are carried out while the PMG moves laterally from the origin [in Fig. 2(b)] to +4 mm, then to −4 mm and finally to +4 mm at WH of 20 mm.

The vertical stiffness measurements were done at two different FCHs of FCH 35–15 and FCH 20–30. After the cooling of the HTSs in related FCHs, the levitation force is measured depending on vertical distance between the upper surface of the PMG and the bottom of the upper HTSs. The vertical magnetic stiffness values are determined by making minor loops on the major levitation force curves at the certain vertical heights of $z =$ 5, 9, 13, and 17 mm, and the vertical loop of $\Delta z = \pm 2$ mm [34].

2) *Dynamic Measurements*

The dynamic response characteristics of multisurface Halbach HTS–PMG arrangement such as resonance frequency and dynamic stiffness were determined with the dynamic experimental setup given in Fig. 3. Firstly, the handmade cryostat was placed over the Halbach PMG symmetrically in x- and y-axis {see Fig. 3(a)}, then HTSs were cooled via liquid nitrogen in three different FCHs [shown in Fig. 3(a)] of 5, 7, and 10 mm above the Halbach PMG to investigate the relationship between the dynamic response characteristics and FCH. After the cooling procedure, the cryostat with total mass of 6.23 and 6.57 kg, respectively for SS–2 HTS and MS–4 HTS arrangements (including the HTSs and liquid nitrogen), released to levitate freely above the Halbach PMG and an impulse force was applied by a hammer (PCB model–086C03) to points A and B in Fig. 3(b) to trigger an oscillation for vertical and lateral dynamic excitations, respectively. The free vibration signals were taken via NI–9234 4–Channel 24–Bit vibration input module equipped with B&K triaxial accelerometer (model 4524–B) and the vibration signals were analyzed via NI LabVIEW 2011 Signal Express module. The vertical and lateral displacement of the cryostat including 6 HTS sample was read by Baumer OM70 laser displacement sensors in z- and x-axis.

III. Theoretical Modeling

In this section, we outline the theoretical framework that has been used to provide a physical interpretation of the force–displacement characteristics of the system.

It is well established that the hysteretic behavior of levitation systems with permanent magnets and high–T_c bulks is well captured by assuming 1) uniformly magnetized permanent magnets and 2) the critical state regime (or a steep E(J) power–law) for the superconductors. In fact, as recently compiled in [28] 2-D and 3-D protocols that combine dedicated experimental calibrations and simulation software are known. These procedures have been successfully applied to single-surface HTS–PMG arrangements and rely on the determination of some set of material parameters that characterize the HTS bulk. In our case, being focused on the description of the multisurface system, we have developed a single-parameter model, based on the critical state description introduced in [35]. As seen below, this "minimal" description allows to capture the physical implications of the multisurface concept with the least mathematical and numerical complication, allowing very reasonable predictions.

Following the ideas and notation introduced in [35], we will describe our experiments in the following terms. To start with, keeping in mind that the real problem is 3-D in nature, an important modeling simplification will be made in order to make it more tractable. We will assume that the system is infinite along the y-axis, thus giving place to a 2-D statement. It is remarkable that this seemingly simplified ansatz will capture the relevant physics of the problem, not only leading to foretell the correct qualitative behavior, but also enable to provide reasonable quantitative estimates. Nevertheless, as expected, the success of the model strongly relies on a careful experimental performance. As the theory takes up translational symmetry along the y-axis, attention had to be paid to the arrangement of the experimental setup. Symmetric collocation respect to the XZ plane $y = 0$ was mandatory.

The Halbach array will be described as the superposition of five blocks (long bars along y-axis) with uniform magnetization

values given by

$$\begin{aligned} \boldsymbol{M}_1 = & - \boldsymbol{M}_3 = \boldsymbol{M}_5 = M_0\, \hat{\boldsymbol{x}} \\ \boldsymbol{M}_2 = & - \boldsymbol{M}_4 = M_0\, \hat{\boldsymbol{z}}. \end{aligned} \tag{3.1}$$

Thus, each of them is equivalent to two layers of current obtained from

$$\boldsymbol{K}_{\rm i} = \boldsymbol{M}_i \times \hat{\boldsymbol{n}}. \tag{3.2}$$

$\hat{\boldsymbol{n}}$ being the unit vector normal to the surface. For instance, one has ${\boldsymbol{K}_1}^{\rm up} = -M_0\, \hat{\boldsymbol{y}}$ and ${\boldsymbol{K}_1}^{\rm down} = M_0\, \hat{\boldsymbol{y}}$, respectively, at the upper/lower surfaces of the left-most magnet named 1. The full set of surface current layers, discretized by $N_{\rm M}$ individual wires along the bars, will be denoted by the finite element vector $|{\rm K_M}\rangle$.

Concerning the superconducting blocks, each of them will be described by a grid of parallel wires across the full section, along the *y*-axis, each carrying a current density with maximum value J_c, according to the critical state ansatz. Also, we define a full set finite element vector $|{\rm J}\rangle$, that will store the values of the actual critical current density at the superconducting "wires" ($J_i, i = 12, \ldots N_{\rm SC}$) with $N_{\rm SC}$ the full number of elementary superconducting wires. By contrast to the magnetization currents, $|{\rm J}\rangle$ represents the set of unknowns to be solved and may be obtained by incrementally updating along the given process, defined by some cooling position and trajectory of the magnets. Specifically, assuming that the solution is known for a given configuration, say $|{\rm J}^{\vee}\rangle$, the updated solution for a small displacement is obtained from the variational principle (equivalent to Faraday's law)

$$\text{minimize} \left[\frac{1}{2} \langle {\rm J}\, |{\rm m}|\, {\rm J}\rangle - \langle {\rm J}^{\vee}\, |{\rm m}|\, {\rm J}\rangle + \langle {\rm A}_M - {\rm A}_M^{\vee} | {\rm J}\rangle \right]. \tag{3.3}$$

Here, we have introduced the mutual induction matrix ${\rm m}$ and the magnet's vector potential $|{\rm A_M}\rangle$. The former contains the coefficients that couple the superconducting circuits (long wires), whereas the latter is an array containing the vector potential created by the magnetization currents $|{\rm K_M}\rangle$ at the points of the superconducting mesh. As before, the notation $|{\rm A}_M^{\vee}\rangle$ represents the vector potential for the previous position of the magnets.

On the other hand, minimization must be performed under a set of restrictions

$$\begin{aligned} J_i \le J_c \,\forall\, i &= 1, 2, \ldots N_{\rm SC} \\ \sum_{i\,\in\,\text{Block}} J_i = 0 \,\text{Block} &= \#1, \#2, \ldots \#6 \cdot \end{aligned} \tag{3.4}$$

The first condition is the critical state ansatz. The second one indicates that within each superconducting block, currents flow as loops, and thus, they should add to zero in the midplane $y = 0$.

Concerning the physical interpretation of (3.3) and (3.4) in terms of the superconducting's material law, one should recall that a strong pinning superconductor is assumed (as corresponds to the high J_c values of our YBCO bulks). In particular, based on this, one may implement the field cooling condition (FCH) just by starting the process with the given vector potential of the magnets and $|{\rm J}^{\vee}\rangle = 0$. This means that upon cooling down from above $T_{\rm c}$, a frozen (pinned) profile of magnetic field (created by the magnet's) is the starting point of the process.

The solution of (3.3) and (3.4) for a given experimental process is done as follows. A certain "magnetization" sequence will be defined by an array of positions for the magnets and thus of values for the vector potential at the superconducting blocks: ${\rm A}_M^0 \to {\rm A}_M^1,\ {\rm A}_M^2,\ {\rm A}_M^3,\ \ldots$. From these, and by sequential application of the minimization equation, we obtain a set of values for the superconducting current density distributions $|{\rm J}^1\rangle,\ |{\rm J}^2\rangle, |{\rm J}^3\rangle,\ \ldots$. With this information at hand, one may characterize the electromechanical response of the system by further exploiting the physical picture of equivalent current circuits. Thus, the force between the magnets and superconductors may be evaluated by summation over the elementary expression

$$f_{\alpha i} = \mu_0\, M_0 \delta_M J_c \delta\, \frac{J_i}{2\pi} \frac{(x_i - x_\alpha, 0, z_i - z_\alpha)}{(x_i - x_\alpha)^2 + (z_i - z_\alpha)^2} \tag{3.5}$$

that gives the force per unit length between the equivalent α–wire of magnetization and the i–th superconducting wire, that carries a normalized current density J_i. Here, $\delta_{\rm M}$ and δ denote the width of the elementary magnetic and superconducting wires' cross sections used in the discretization process. Eventually, one must perform the summation over the magnetic circuits $\alpha = 1,\ 2, \ldots N_M$ and over the superconducting circuits $i = 1,\ 2, \ldots N_{\rm SC}$. Quantitative values of the force are obtained by using the actual values of the material parameters M_0 and J_c , and the specific dimensions of the system. In particular, this entails multiplying the force obtained via (3.5) by the length of our blocks along the *y*-axis so as to get an approximation to the real facts from our 2-D approximation.

In order to gain physical insight, we have also used the plots of magnetic field lines, as shown in Fig. 4. For this, we recall the property that in 2-D systems they coincide with the contour levels of the vector potential $\boldsymbol{A}$, and the relation $|A\rangle = |{\rm A_M}\rangle + |{\rm A_{SC}}\rangle$ that gives the vector potential at the points of the finite element mesh. To the left of the figure, we show the situation above the superconducting critical temperature. Only the magnets contribute and, thus, we obtain the magnetic field structure expected for the Halbach arrangement. To the right, we show the result of first cooling the superconductor in that configuration and then pushing the PMG upward. Supercurrents are induced and the subsequent field profile noticeably differs from the magnets. Notice that the superconductor creates a flux trapping effect, i.e., the HTS blocks are penetrated by currents (not shown) that try to retain the original flux structure within them.

IV. Results and Discussion

A. Experimental Results

1) Levitation Force: As it is well established, the HTS–PMG combination should be optimized to achieve not only larger levitation force but also larger guidance force to provide magnetic stability together while decreasing all fabrication cost of Maglev systems. Although some advancements have been achieved on improving the levitation or guidance force and related stiffness efficiency of YBCOs separately, these properties could not be

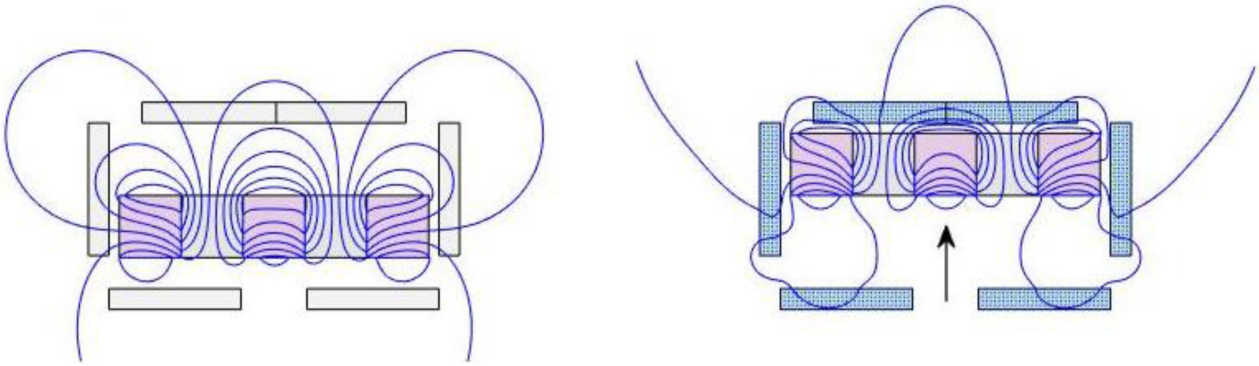

Fig. 4. To the left we show the magnetic field lines of the Halbach array ($T > T_c$). To the right we show the configuration after cooling the superconducting blocks and then pushing up the magnets.

improved simultaneously by using the single-surface Halbach or other HTS–PMG arrangements [30], [33]. Therefore, a new multisurface Halbach HTS–PMG arrangement has been designed in this study and the levitation force, guidance force, and magnetic stiffness measurements were performed in different FCHs to determine the optimum electromagnetic properties of Maglev systems while decreasing the fabrication cost. It is known that by conception, most of the magnetic flux density is concentrated on the upper surface of Halbach PMG [30]. Although it can be predicted that the lower HTSs (see Fig. 2) make minor contribution to the levitation force in Halbach HTS-PMG arrangement, we have used MS-6 HTS arrangement in addition to the SS-2 HTS and MS-4 HTS arrangements in order to show the consistency of theoretical expectations and experimental results. In fact, according to the magnetic line structure in Fig. 4 a certain (subtle) influence of the lower blocks that trap a certain amount of flux could be expected.

Fig. 5 shows the levitation force curves of novel multisurface Halbach HTS–PMG arrangement with MS–6 HTS, MS–4 HTS (b), and SS–2 HTS (c) in different FCHs. The maximum levitation force values, at the minimum vertical gaps of 5 mm, for MS–6 HTS arrangement were obtained as 339.7, 345.5, and 78.3 N in FCH 35–15, FCH 20–30, and FCH 5–45 procedures, respectively. One can see from Fig. 5(a) that the levitation force values in FCH 35–15 case are bigger than that of FCH 20–30 case at bigger vertical distances of z. The negative force values of MS–6 HTS and MS–4 HTS in FCH 20–30 case at the vertical distance of 20–35 mm result from the trapped flux inside the HTSs during the cooling procedure due to optimum electromagnetic interaction between the magnetic flux distribution of Halbach PMG and the HTSs in this FCH [29]. The absence of similar situation for SS–2 HTS arrangement [Fig. 5(c)] can be attributed to effect of the HTSs at sides of the cryostat in multisurface arrangements. As seen in Fig. 5, the increasing maximum negative force values in FCH 5–45 from about -125 to -200 N with increasing HTS number indicates the effect of side HTSs on the pinning force properties of whole system. This situation is already an indication that the stability properties (related to the flux trapping effects) of Maglev systems can be improved by using multisurface HTS-PMG arrangements.

In a recent study a single-surface Halbach HTS–PMG arrangement with eight YBCO prisms of dimensions of 64 mm $\times$ 32 mm $\times$ 13 mm were used and a maximum levitation force of 533.4 N was obtained at the minimum vertical gap of 10 mm, in FCH $=$ 20 mm and at the measurement temperature of 80 K [36]. Besides, three sets of Halbach PMG were used when the length of a PM is taken as about 40 mm, and it was observed that the levitation force increases with decreasing measurement temperature. The levitation force increases with increasing FCH, but operational vertical working gap of Maglev systems can be accepted as 20 mm in practical applications to ensure optimum vertical stability and loading capacity of vehicle. As for the multisurface Halbach HTS–PMG arrangement with 4 HTS in our study for only one set of PMG (the length of each PM is 40 mm), a maximum levitation force of 171.6 N (in addition to a maximum attractive force of -82 N at vertical gap of 35 mm) was obtained at the vertical gap of 10 mm and FCH 20–30 case at 77 K {see Fig. 5(b)}. Thus, it can be expected that the maximum levitation force will be tripled as 514.8 N when three sets of Halbach PMG is used with multisurface HTS–PMG arrangement and the levitation force values of this study is compatible with the literature [36] although the measurement procedures are a bit different.

2) Guidance Force: It is known that the lateral guidance force is an important parameter for Maglev systems, since the movement stability of Maglev systems can be enhanced by improving lateral guidance force properties. Fig. 6 shows the guidance force comparisons of MS–6 HTS, MS–4 HTS, and SS–2 HTS arrangements in FCH 5–45 and FCH 20–30 cases. The maximum guidance force values were obtained as -60.4, -59.7, -15.2 N, respectively for MS–6 HTS, MS–4 HTS, and SS–2 HTS arrangements in FCH 5–45 and respectively as -45.2, -48.5, and -3.6 N in FCH 20–30. It can be seen by comparing Fig. 6(a) and (b) that the multisurface arrangements have bigger guidance force values than single surface one in both FCH. Nearly four times bigger guidance force values of MS–6 HTS and MS–4 HTS arrangements than that of SS–2 HTS arrangement in FCH 5–45 (and more than ten times in FCH 20–30) indicates that the side HTSs in multisurface arrangements make a significant contribution to the guidance force and thus the lateral movement stability of Maglev systems. In addition,

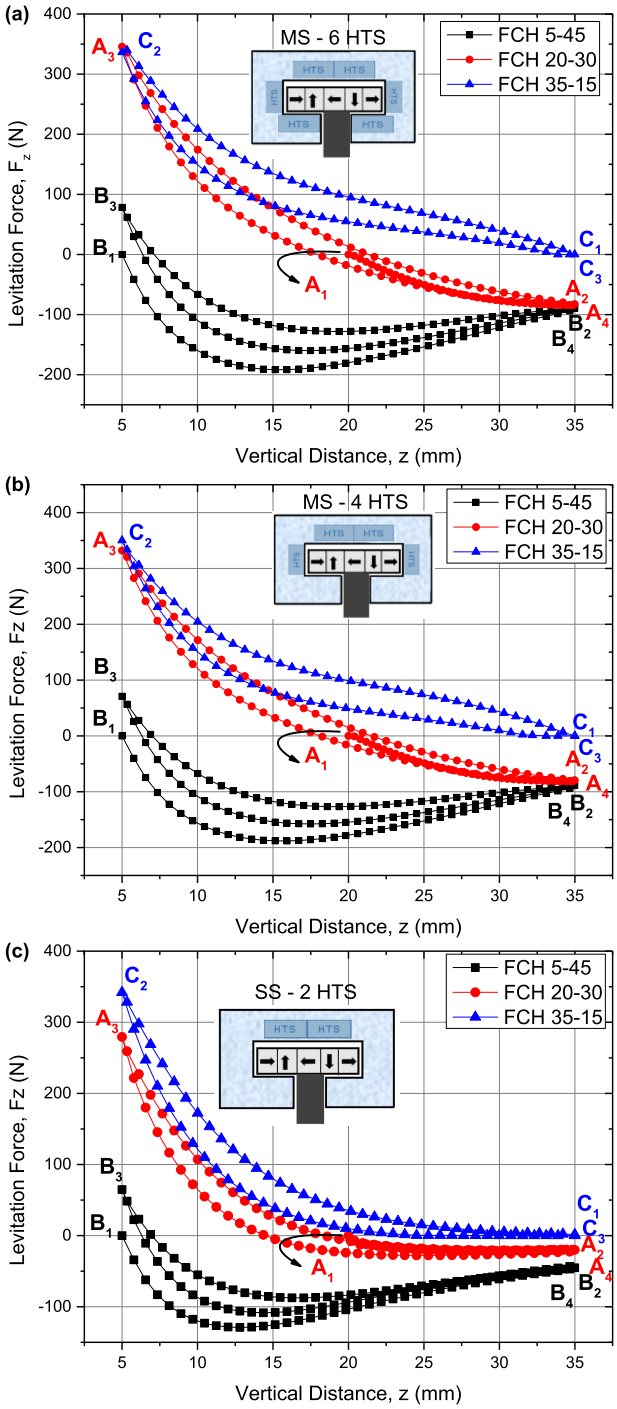

Fig. 5. Levitation force curves of novel multisurface Halbach HTS–PMG arrangement in different FCHs with (a) MS–6 HTS, (b) MS–4 HTS, and (c) SS–2 HTS configurations.

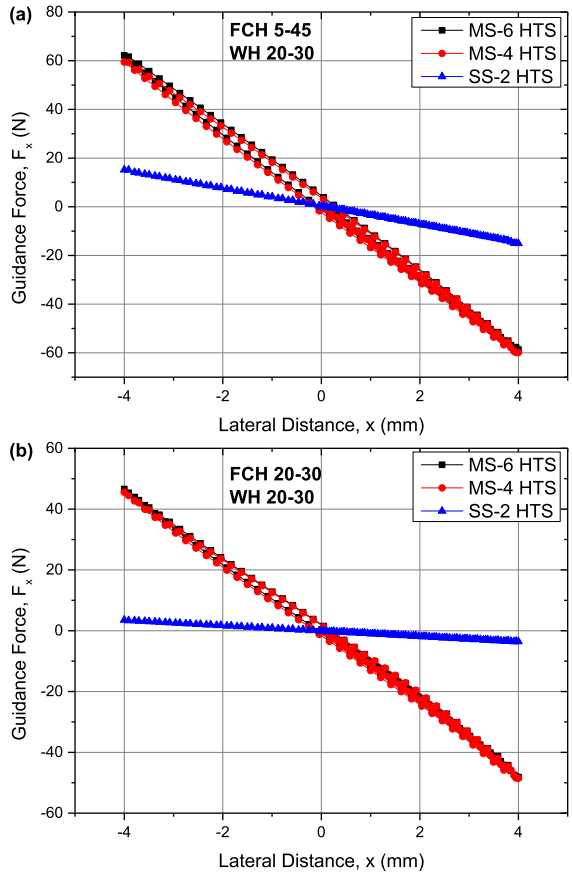

Fig. 6. Guidance force of multisurface Halbach HTS–PMG arrangement with MS-6 HTS, MS-4 HTS and SS–2 HTS in (a) FCH 5–45 and (b) FCH 20–30 cases at WH 20–30.

the bigger negative levitation force values of MS–6 HTS and MS–4 HTS arrangements in Fig. 5(a) and (b) than that of SS–2 HTS arrangement especially at the vertical gap between 25 and 35 mm indicates that the side HTSs contribute to the vertical stability as well as to the lateral stability.

3) Stiffness: The magnetic stiffness is an important parameter for stability of Maglev systems. Recall that the vertical magnetic stiffness is defined as $k_z = -\frac{\partial F_z}{\partial z}\ (Nmm^{-1})$, where, F_z is the levitation force and z is the levitation gap [23]. Fig. 7 shows the experimental vertical magnetic stiffness of the MS–6 HTS, MS–4 HTS, and SS–2 HTS arrangements in FCH 20–30 case. It is seen in Fig. 7 that the vertical magnetic stiffness values of all arrangements increase with decreasing vertical distance. This can be attributed to the fact that the levitation force curve increases more rapidly at smaller vertical distances, as can be seen in Fig. 5, since the magnetic stiffness is derivative of the levitation force with respect to the vertical position. As can be seen in this figure, the stiffness values of MS–6 HTS and MS–4 HTS arrangements are almost identical within the error limitations of the measurement system. Besides, as distance increases also does the difference between the magnetic stiffness of single- and multiple-surface systems. Again, one may say that the electromagnetic interaction is enhanced by the superconductors at the left and right sides.

4) Dynamic Behavior: In addition to the static parameters such as levitation force, guidance force, and magnetic stiffness, the dynamic vibration parameters are also important for movement stability of Maglev systems. Having observed this, as expected, the behavior of the MS-6 HTS and MS-4 HTS arrangements is nearly undistinguishable (Fig. 5), the dynamic behavior was only focused on the SS–2HTS and MS–4 HTS arrangements in this study. After an impulse in vertical and

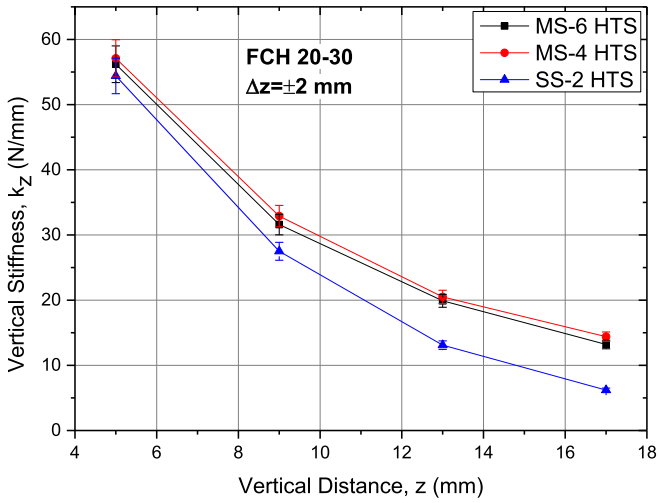

Fig. 7. Vertical magnetic stiffness of multisurface Halbach HTS-PMG arrangement with MS-6 HTS, MS-4 HTS, and SS-2 HTS arrangements.

lateral directions was applied to respectively point A and point B shown in Fig. 3(b), the free cryostat oscillates in the vertical and lateral directions as described by the following equations:

$$m\ddot{z} + c_z\dot{z} + k_{zD}z = 0$$
$$m\ddot{x} + c_x\dot{x} + k_{xD}x = 0 \quad (4.1)$$

where z, c_z, k_{zD} and x, c_x, k_{xD} represent the displacement of the levitated cryostat, damping coefficient, dynamic stiffness in vertical and lateral directions, respectively, while m represents the total mass of the multisurface cryostat including HTSs. The dynamic stiffness in vertical and lateral directions are calculated as follows according to the (4.1):

$$w_n = \sqrt{k/m}, \quad k = m(2\pi f)^2 \quad (4.2)$$

where f represents the resonance frequency.

The suspension distance between onboard HTS unit and PMG in superconducting Maglev systems is an important parameter for stable and safe movement of the vehicle. Fig. 8 shows the frequency-domain response of MS–4 HTS arrangement in different FCHs of 5, 7, and 10 mm, after the pulse force was applied by the hammer to point A and point B in Fig. 3(b), respectively, on the vertical direction and lateral directions. The averaged vertical vibration displacement at the time interval of 0–2 s was determined from data processing of the acceleration as 0.75 mm for all FCH situations and this situation indicates the safety of the system. The vertical resonance frequencies were determined as 17.5, 15.4, and 13.5 Hz, respectively, in FCH = 5, 7, and 10 mm, while lateral resonance frequencies were determined as 9.7, 9.5, and 9.4 Hz. These results are comparable with the literature [1] in which the vertical and lateral resonance frequencies were determined respectively as 17.8 Hz and about 5.5 Hz between the Halbach PMG arrangement and single-surface cryostat of different mass, in FCH = 15 mm. The vertical and lateral dynamic stiffness of MS–4 HTS and SS–2 HTS arrangements, calculated from (2) are shown in Fig. 9 depending on FCH. The maximum vertical dynamic

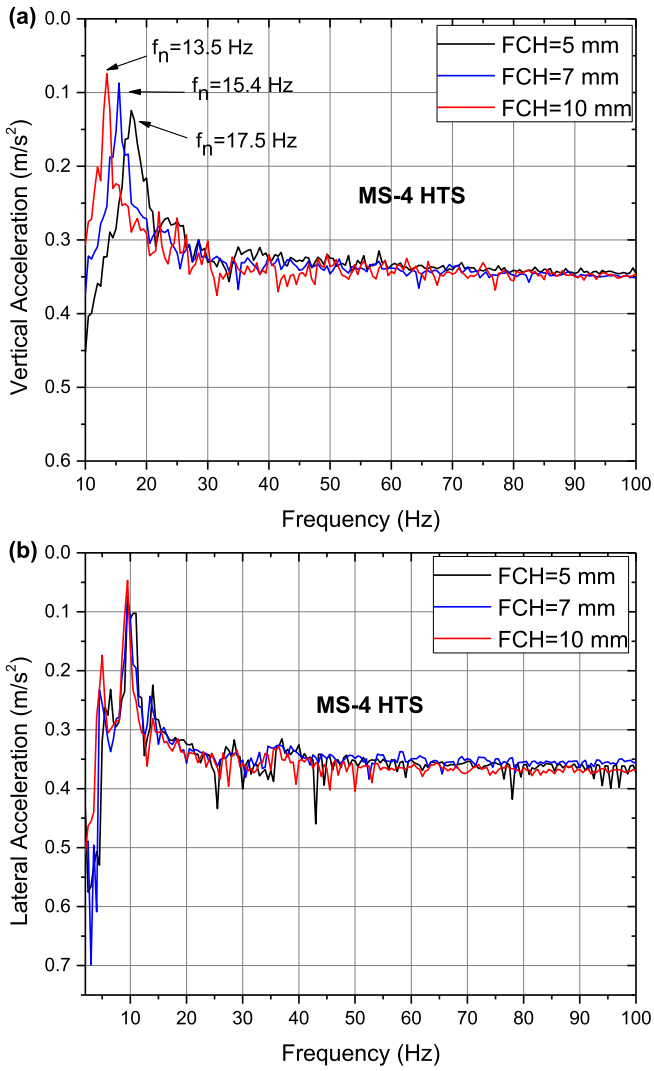

Fig. 8. Frequency-domain response of MS–4 HTS arrangement in different FCHs, after the pulse force was applied by the hammer at point A and point B in Fig. 3, respectively, on (a) the vertical direction and (b) the lateral direction.

stiffness values of MS–4 HTS and SS–2 HTS arrangements were determined in minimum FCH of 5 mm as 79.4 and 76.4 N/mm, respectively, while the lateral dynamic stiffness values were determined respectively as 24.4 and 21.8 N/mm. It can be said from this figure that both the vertical and lateral dynamic stiffness values increase with decreasing FCH. As said before, the bigger dynamic stiffness in small FCHs can be attributed to larger electromagnetic interaction density, due to the bigger magnetic flux density of PMG and its gradient, between the PMG and onboard HTS unit in multisurface HTS–PMG arrangement. The vertical and lateral dynamic stiffness values of MS–4 HTS arrangement respectively dropped from 79.4 to 47.3 N/mm and from 24.4 to 22.9 N/mm with increasing FCH from 5 to 10 mm. This corresponds to 40.4 and 6.1% decrement, respectively for the vertical and lateral dynamic stiffness values. On the other hand, the drop was observed as 42.9% in vertical dynamic stiffness and 50.5% in lateral dynamic stiffness of SS–2 HTS arrangement. One can see that the drop ratio of MS–4 HTS

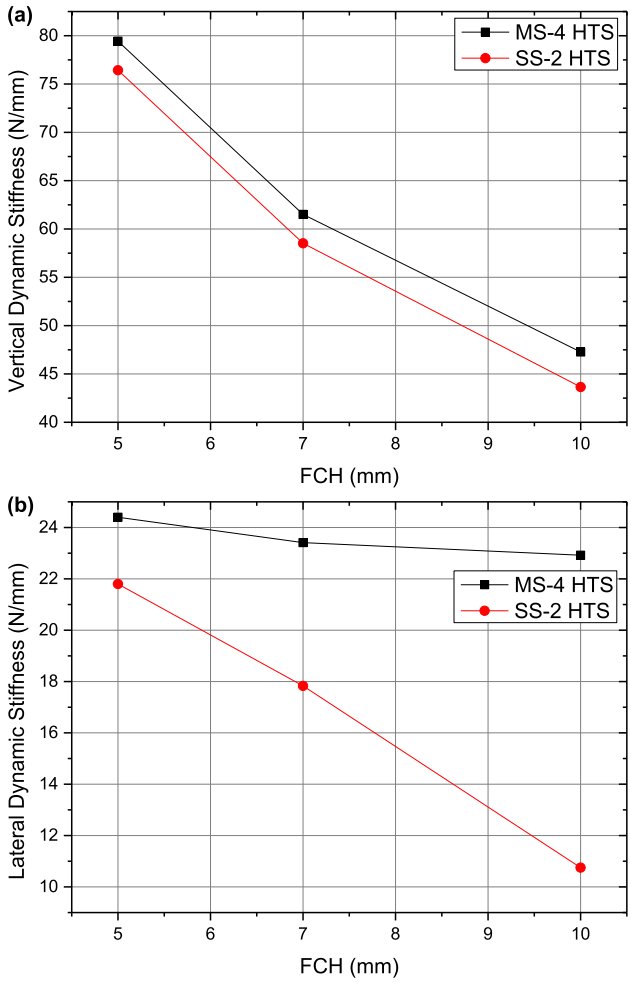

Fig. 9. (a) Resonance frequency and (b) dynamic stiffness of MS-4 HTS and SS-2 HTS arrangements depending on FCH.

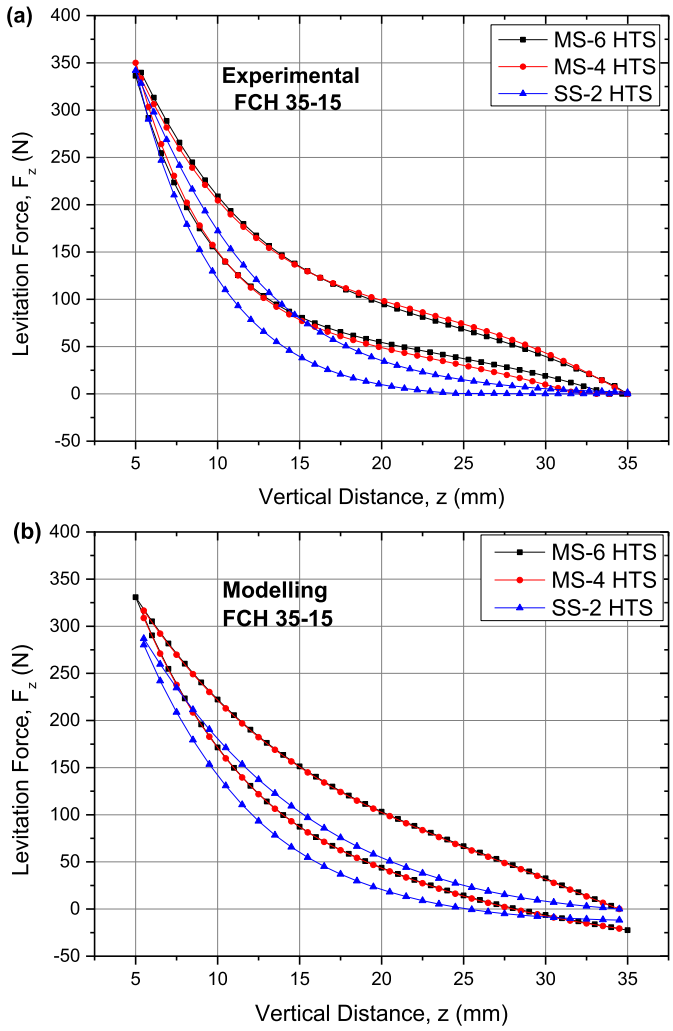

Fig. 10. Comparison of the magnetic levitation force of the multisurface Halbach HTS-PMG arrangements with MS-6 HTS, MS-4 HTS, and SS-2 HTS in FCH 35-15 case. (a) Experimental measurements. (b) Theoretical modeling.

and SS–2 HTS arrangements are close to each other in vertical direction while the drop ratio in lateral dynamic stiffness of SS–2 HTS arrangement is more than 8 times bigger than that of MS–4 HTS arrangement. This situation indicates that the HTSs at the left and right sides in MS–4HTS arrangement compensate the dynamic stiffness decay in multisurface arrangements, which is necessary for the lateral movement stability of HTS Maglev systems.

B. Processing of Results: Model and Experiments

In this section, we analyze the electromechanical response of the system for the different processes described in the experimental procedure. We must mention that the actual value of the main (single in fact) parameter of the model, i.e., the critical current density J_c, as well as the dependence of this parameter on the local magnetic field have been considered and investigated. In view of the moderate influence of such dependence in our study and aiming at the least mathematical complication for the model, we have eventually used Bean's hypothesis of constant J_c as a basic physical picture of the system. This simplifies the description of the superconducting bulks to a single parameter model. We have taken the value $J_c = 1.33\ 10^8 \mathrm{A/m}^2$ as a reasonable average, according to the values reported in the literature [13] for magnetic fields in the range of 0.5 T (typical flux density at the magnets' surface).

1) Levitation Force: Below, we present the comparison between experiments and modeling results both for the levitation and guidance forces in different FCH cases.

The FCH 35-15 case is shown in Fig. 10(a) and (b), respectively. In Fig. 10(a), it may be seen that the maximum values and curve behavior of MS–6 HTS and MS–4 HTS arrangements are nearly coincident and the SS–2 HTS arrangement separates from the others in terms of full curve behavior. The reason of the similar behavior of MS–6 HTS and MS–4 HTS arrangements is that in practice, the lower HTSs (HTS 5 and HTS 6 in Fig. 2) do not contribute noticeably to the levitation force of the system, owing to the upper position of the magnetic pole positions of Halbach PMG as related to Figs. 2 and 4. Besides, as seen in Fig. 10(a), the bigger levitation force of MS–6 HTS and MS–4 HTS arrangements at the far vertical gaps between 20–30 mm as compared to the single surface SS–2 HTS arrangement indicates

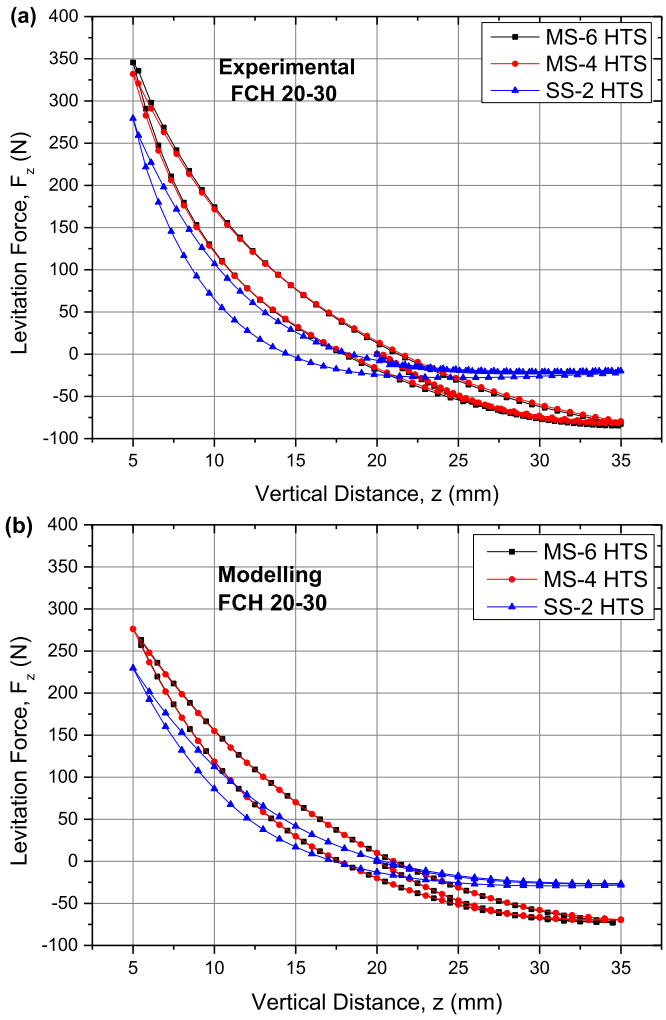

Fig. 11. Comparison of the magnetic levitation force of the multisurface Halbach HTS-PMG arrangements with MS-6 HTS, MS-4 HTS, and SS-2 HTS in FCH 20-30 case. (a) Experimental measurements. (b) Theoretical modeling.

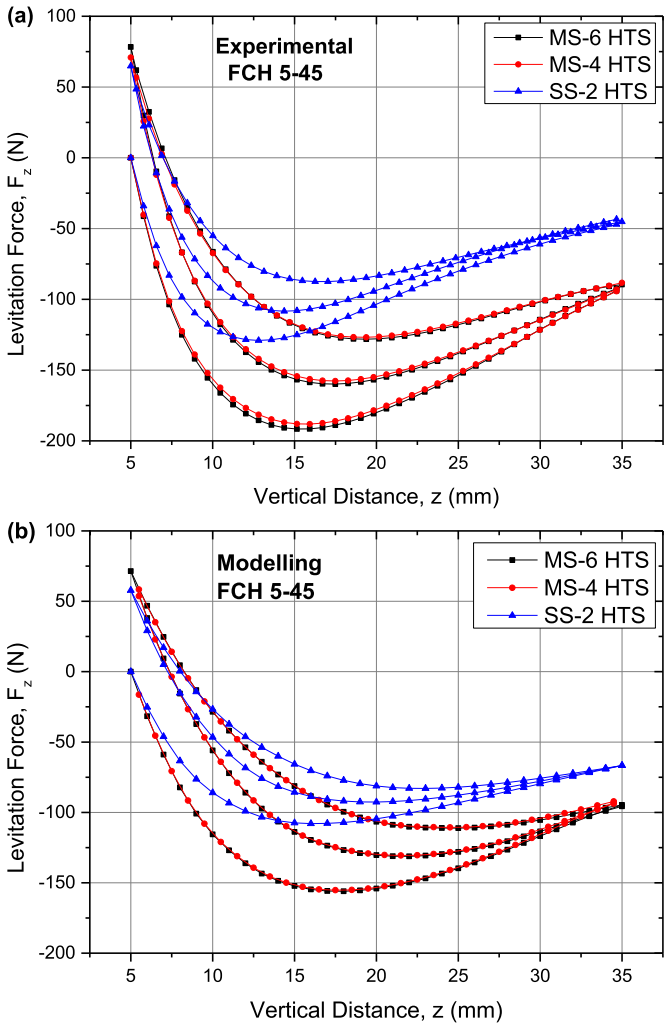

Fig. 12. Comparison of the magnetic levitation force of the multisurface Halbach HTS-PMG arrangements with MS-6 HTS, MS-4 HTS, and SS-2 HTS in FCH 5-45 case. (a) Experimental measurements. (b) Theoretical modeling.

that the multisurface arrangements have bigger vertical loading capacity and wider loading gap than conventional single-surface ones. One may stress that upper/lower flux is not the only relevant question. The role of HTS3 and HTS4 shows that one must be also focused on the importance of lateral flux even with Halbach arrays that concentrate flux upon the PMG.

In Figs. 11 and 12 we compare theory and experiment for the cooling routes named FCH 20-30 and FCH 5-45. Again, one may notice no difference between the MS–6 HTS and MS–4 HTS configurations, while a rather distinctive behavior occurs for SS–2 HTS. Thus, this is a general indication of the relevant role of the superconducting blocks HTS 3 and HTS 4 and of the minor role of 5 and 6 as concerns the levitation force.

We emphasize that as it is clearly seen in Figs. 10–12, the hysteretic behavior of the levitation force curves of our single surface and multisurface arrangements is well captured by the critical state modeling, in particular as concerns the role of the lateral HTS blocks.

2) Guidance Force: Finally, we analyze the guidance force for several configurations that will be compared to the experimental data. Thus, we define the field cooling processes labeled FCH 5–45 and FCH 20–30. Subsequent to this, the PMG is settled at the working height of WH 20–30 [$z = 20$ mm in Fig. 2(b)] and then we simulate the process of horizontal displacements with amplitude $\Delta x \pm 4$ mm. The modeling results for the guidance force induced by the lateral displacements are shown in Fig. 13 and the experimental results are given as inset for comparison. We notice that, again, virtually no difference may be observed in modeling results of the cases MS–6 HTS and MS–4 HTS, while a noticeable reduction is observed for the case SS–2 HTS as compatible with the experimental results. Moreover, although there is some difference between the quantitative values of modeling and experimental results, the hysteresis curve behaviors are very similar.

As it might be expected, the role of the lateral superconducting blocks, i.e., HTS 3 and HTS 4 is very relevant when the guidance force is concerned.

As a final comment of this section, and for the readers' sake we mention that the results presented here were obtained by imposing the restriction (3.4) for the case of the actual superconducting blocks of the experimental system. Nevertheless, treating the upper adjacent blocks HTS 1 and HTS 2 as a single

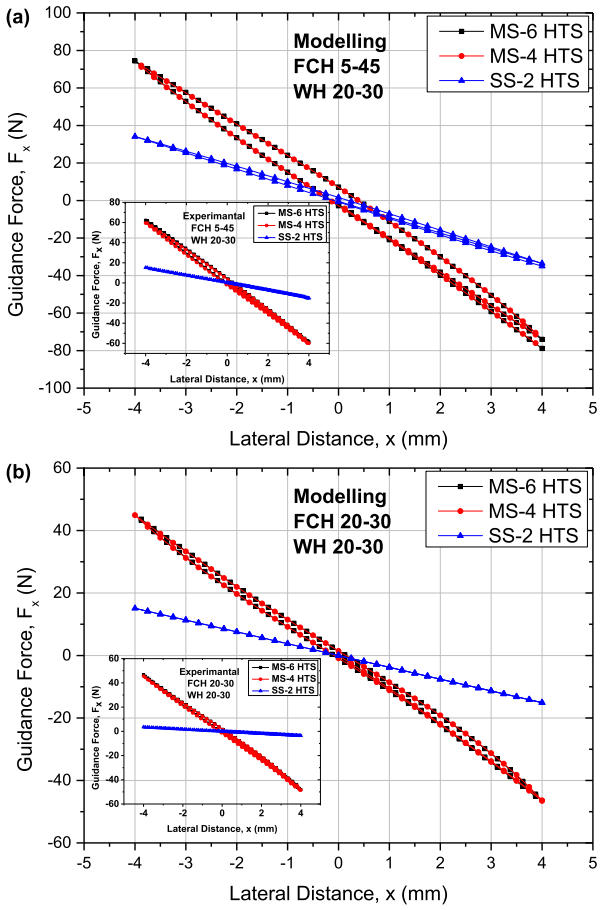

Fig. 13. Comparison of the guidance force of the multisurface Halbach HTS-PMG arrangements obtained from numerical simulations in different cooling conditions of (a) FCH 5-45 and (b) FCH 20-30 for the arrangements of MS-6 HTS, MS-4 HTS, and SS-2 HTS. The insets show the experimental measurements.

one, makes nearly no difference in the vertical forces, while a slight increase of the guidance force is obtained. Physically, the difference relies on the fact that, in fact, superconducting current loops are restricted to circulate within each bulk. For the first case, due to symmetry actual induced current loops are indeed confined within HTS 1 and HTS 2 and no difference arises. However, for the lateral displacements a small benefit could be obtained if an oversized block were used because bigger current loops may circulate across the boundary in $x = 0$ with a related increase in the forces.

V. Conclusion

We have introduced novel multisurface Halbach HTS–PMG arrangements (NdFeB magnets and YBCO monolithic blocks) and investigated 1) static force parameters such as levitation force, guidance force, and magnetic stiffness and 2) dynamic response characteristics such as resonance frequency and dynamic stiffness. Three different Halbach HTS–PMG arrangements with 6 HTS (MS–6 HTS), 4 HTS (MS–4 HTS), and 2 HTS (SS–2 HTS) were used and the static and dynamic measurements were carried out in different FCHs. The 6 HTS and 4 HTS configurations include superconducting blocks both within the "upper" high-flux-density zone of the Halbach array and capping the lateral sides. Our basic findings may be summarized as follows:

1) By testing at extremal cooling positions allowed in our system, we obtain the maximum levitation force values of multisurface system for MS–6 HTS arrangement (virtually identical for MS–4 HTS) were 339.7, 345.5, and 78.3 N, respectively, in FCH 35–15, FCH 20–30, and FCH 5–45 cases. They correspond to a decreasing field cooling gap between the magnets and upper superconductors.
2) The bigger levitation force of MS–6 HTS and MS–4 HTS arrangements at the far vertical gaps of 20–30 mm with respect to SS–2 HTS indicates that the multisurface arrangements have bigger vertical loading capacity and wider loading gap than conventional single–surface one.
3) The maximum negative force values attained for the process with cooling height of 5 mm (increasing from -125 to -200 N by adding the lateral blocks indicates the effect of side HTSs on the pinning force properties of whole system.
4) Nearly four times bigger guidance force values of multisurface arrangements of MS–6 HTS and MS–4 HTS (about -60 N) as compared to that of single-surface one (-15 N) indicates that the side HTSs make a significant contribution to the guidance force and thus the lateral movement stability of Maglev systems.
5) The 2 HTSs at the sides in multisurface MS–4HTS arrangement diminish the lateral dynamic stiffness drop ratio more than eight times as compared to the SS–2HTS arrangement. Again, this is an indication of the stabilizing role of the lateral HTSs.
6) All the experimental observations are satisfactorily explained by a physical model with a single material parameter for the HTS bulks, i.e., the critical current density.

It can be concluded that both the static and dynamic parameters of HTS Maglev systems can be enhanced by using multisurface Halbach HTS–PMG. Taking advantage of this property is thought to be useful for engineering studies on the practical applications of Maglev systems.

Acknowledgment

The authors would like to thank technician L. Demir from the Department of Mechanical Engineering for his help in the experimental setup.

References

[1] B. Wang, J. Zheng, T. Che, B. T. Zheng, S. S. Si, and Z. G. Deng, "Dynamic response characteristics of high temperature superconducting maglev systems: Comparison between Halbach-type and normal permanent magnet guideways," *Physica C: Supercond. Appl.*, vol. 519, pp. 147–152, 2015.
[2] L. Schultz *et al.*, "Superconductively levitated transport system—The supratrans project," *IEEE Trans. Appl. Supercond.*, vol. 15, no. 2, pp. 2301–2305, Jun. 2005.
[3] F. F. Da Silva and P. J. C. Branco, "Study of a cylindrical geometry design for a zero field cooled Maglev system," *Supercond. Sci. Technol.*, vol. 32, 2019. Art. no. 65004.
[4] K. Ozturk, S. B. Guner, M. Abdioglu, M. Demirci, S. Celik, and A. Cansiz, "An analysis on the relation between the seed distance and vertical levitation force for the multi-seeded YBCO using the modified advanced frozen image (MAFI) and experimental methods," *J. Alloys Compounds*, vol. 805, pp. 1208–1216, 2019.

[5] G. G. Sotelo *et al.*, "Experimental and theoretical levitation forces in a superconducting bearing for a real-scale Maglev system," *IEEE Trans. Appl. Supercond.*, vol. 21, no. 5, pp. 3532–3540, Oct. 2011.
[6] H. Huang *et al.*, "Correlations between magnetic flux and levitation force of HTS bulk above a permanent magnet guideway," *J. Low. Temp. Phys.*, vol. 189, pp. 42–52, 2017.
[7] K. Ozturk, M. Abdioglu, E. Sahin, S. Celik, H. Gedikli, and B. Savaskan, "The effect of magnetic field distribution and pole array on the vertical levitation force properties of HTS Maglev systems," *IEEE Trans. Appl. Supercond.*, vol. 25, no. 4, Aug. 2015, Art. no. 3601607.
[8] M. Abdioglu, K. Ozturk, S. Kutuk, S. Bolat, and E. Yanmaz, "Effect of magnetic flux distribution and magnetic powder addition on the magnetic levitation force of Sm123 superconductors," *J. Supercond. Nov. Magn.*, vol. 25, pp. 923–929, 2012.
[9] B. Savaskan, M. Abdioglu, and K. Ozturk, "Determination of magnetic levitation force properties of bulk MgB2 for different permanent magnetic guideways in different cooling heights," *J. Alloys Compounds*, vol. 834, 2020, Art. no. 155167.
[10] E. Yanmaz, K. Ozturk, C. Dancer, M. Basoglu, S. Celik, and C. Grovenor, "Levitation force at different temperatures and superconducting properties of nano-structured MgB2 superconductors," *J. Alloys Compounds*, vol. 492, pp. 48–51, 2010.
[11] B. Savaskan, S. B. Guner, A. Yamamoto, and K. Ozturk, "Trapped magnetic field and levitation force properties of multi-seeded YBCO superconductors with different seed distance," *J. Alloys Compounds*, vol. 829, 2020, Art. no. 154400.
[12] K. Ozturk *et al.*, "IR laser line scanning treatments to improve levitation forces in Mgti0.06B2 bulk materials," *J. Alloys Compounds*, vol. 811, 2019, Art. no. 151966.
[13] J. Zou *et al.*, "Numerical simulation and analysis of single grain YBCO processed from graded precursor powders," *Supercond. Sci. Technol.*, vol. 28, 2015, Art. no. 035016.
[14] N. Del-Valle, A. Sanchez, C. Navau, and D.-X. Chen, "Magnet guideways for superconducting maglevs: Comparison between Halbach-type and conventional arrangements of permanent magnets," *J. Low Tem. Phys.*, vol. 162, pp. 62–71, 2011.
[15] K. Ozturk *et al.*, "Comparative study of the magnetic stiffness, levitation and guidance force properties of single and multi seeded YBCOs for different HTS–PMG arrangements," *J. Alloys Compounds*, vol. 643, pp. 201–206, 2015.
[16] M. Abdioglu, K. Ozturk, S. B. Guner, S. Celik, and T. Kucukomeroglu, "Investigation of magnetic force properties between different PMGs and multi-seeded YBCO superconductors with different seed distances," *Physica C: Supercond. Appl.*, vol. 565, 2019, Art. no. 1353519.
[17] Y. Li, J. Zheng, J. Li, J. Zhang, Y. Zhang, and Z. Deng, "Design optimization and experimental verification of an electromagnetic turnout for HTS Maglev systems," *IEEE Trans. Appl. Supercond.*, vol. 28, no. 4, pp. 1–5, Jun. 2018.
[18] Z. Deng, J. Wang, J. Zheng, Y. Zhang, and S. Wang, "An efficient and economical way to enhance the performance of present HTS Maglev systems by utilizing the anisotropy property of bulk superconductors," *Supercond. Sci. Technol.*, vol. 26, 2013, Art. no. 25001.
[19] F. Cai, J. Liu, D. Zhou, L. Zhao, Y. Zhang, and Y. Zhao, "Optimal YBCO bulk size to maximize running speed of the SS-HTS Maglev circular track system by static simulation experiments," *IEEE Trans. Appl. Supercond.*, vol. 30, no. 3, pp. 1–5, Apr. 2020.
[20] Y.-X. Guo, W.-M. Yang, J.-W. Li, L.-P. Guo, L.-P. Chen, and Q. Li, "Effects of vertical temperature gradient on the growth morphology and properties of single domain YBCO bulks fabricated by a new modified TSIG technique," *Cryst. Growth Des.*, vol. 15, pp. 1771–1775, 2015.
[21] F. N. Werfel *et al.*, "Superconductor bearings, flywheels and transportation," *Supercond. Sci. Technol.*, vol. 25, 2012, Art. no. 14007.
[22] S. B. Güner, M. Abdioğlu, K. Öztürk, and Ş. Çelik, "The comparison of levitation and lateral force of bulk and cut-pasted bulk GdBCO samples at different temperatures," *J. Alloys Compounds*, vol. 822, 2020, Art. no. 153637.
[23] J. R. Hull and A. Cansiz, "Vertical and lateral forces between a permanent magnet and a high-temperature superconductor," *J. Appl. Phys.*, vol. 86, pp. 6396–6404, 1999.
[24] M. D. Ainslie and H. Fujishiro, "Modelling of bulk superconductor magnetization," *Supercond. Sci. Technol.*, vol. 28, 2015, Art. no. 53002.
[25] I. Yildizer, A. Cansiz, and K. Ozturk, "Optimization of levitation and guidance forces in a superconducting Maglev system," *Cryogenics*, vol. 78, pp. 57–65, 2016.
[26] K. Ozturk and C. Dancer, "Electromagnetic behaviour of bulk MgB2 determined by numerical modelling using regional supercurrent properties," *J. Alloys Compounds*, vol. 693, pp. 1109–1115, 2017.
[27] A. Morandi *et al.*, "The measurement and modeling of the levitation force between single-grain YBCO bulk superconductors and permanent magnets," *IEEE Trans. Appl. Supercond.*, vol. 28, no. 5, pp. 1–10, Aug. 2018.
[28] L. Quéval, K. Liu, W. Yang, V. M. R. Zermeño, and G. Ma, "Superconducting magnetic bearings simulation using an H-formulation finite element model," *Supercond. Sci. Technol.*, vol. 31, 2018, Art. no. 84001.
[29] K. Ozturk, M. Kabaer, M. Abdioglu, A. Patel, and A. Cansiz, "Clarification of magnetic levitation force and stability property of multi-seeded YBCO in point of supercurrent coupling effect," *J. Alloys Compounds*, vol. 689, pp. 1076–1082, 2016.
[30] K. Halbach, "Application of permanent magnets in accelerators and electron storage rings (invited)," *J. Appl. Phys.*, vol. 57, pp. 3605–3608, 1985.
[31] S. Basaran and S. Sivrioglu, "Radial stiffness improvement of a flywheel system using multi-surface superconducting levitation," *Supercond. Sci. Technol.*, vol. 30, 2017, Art. no. 35008.
[32] K. Ozturk, M. Abdioglu, and Z. Karaahmet, "Magnetic force and stiffness performances of Maglev system based on multi–surface arrangements with three-seeded bulk YBaCuO superconductors," *Physica C*, vol. 578, 2020, Art. no. 1353739.
[33] M. Abdioglu, K. Ozturk, H. Gedikli, M. Ekici, and A. Cansiz, "Levitation and guidance force efficiencies of bulk YBCO for different permanent magnetic guideways," *J. Alloys Compounds*, vol. 630, pp. 260–265, 2015.
[34] K. Ozturk, M. Kabaer, and M. Abdioglu, "Effect of onboard PM position on the magnetic force and stiffness performance of multi-seeded YBCO," *J. Alloys Compounds*, vol. 644, pp. 267–273, 2015.
[35] A. Badia-Majos, A. Aliaga, J. Letosa-Fleta, M. M. Alfonso, and J. P. Roche, "Tradeoff modeling of superconducting levitation machines: Theory and experiment," *IEEE Trans. Appl. Supercond.*, vol. 25, no. 4, Aug. 2015, Art. no. 3601810.
[36] S. Sun, Z. Deng, G. Wang, L. Wan, and J. Zheng, "Levitation performance of an onboard high-temperature superconducting bulk unit with cryocooler direct cooling," *Supercond. Sci. Technol.*, vol. 33, 2020, Art. no. 94015.

Kemal Ozturk received the B.S. degree in physics education from Marmara University, Istanbul, Turkey, in 1998, and the M.S. and Ph.D. degrees in physics from Karadeniz Technical University (KTU), Trabzon, Turkey, in 2003 and 2006, respectively.

He spent a postdoctoral period with the University of Cambridge, Cambridge, U.K., in 2010, and the University of Warwick, Coventry, U.K., in 2015. He is currently a Professor with the Department of Physics, Scientific Area of Solid State Physics, Institute of Science, KTU. His research interests include electromagnetic force measurements, analytical and numerical simulation, and high-temperature superconducting Maglev applications.

Antonio Badía Majós received the bachelor's and Ph.D. degrees in physics from the University of Zaragoza, Zaragoza, Spain, in 1989 and 1993, respectively.

He is currently a Tenured Professor with the Department of Condensed Matter Physics, School of Engineering and Architecture, University of Zaragoza. His research interests include modeling and simulation of electromagnetic properties of superconducting materials.

Murat Abdioglu received the B.S. degree in physics education and the M.S. and Ph.D. degrees in physics from Karadeniz Technical University, Trabzon, Turkey, in 2008, 2011, and 2015, respectively.

He is currently an Associate Professor with the Department of Mathematics and Science Education, Bayburt University, Bayburt, Turkey. His research interests include superconducting materials, magnetic levitation applications, and high-temperature superconducting Maglev system design.